JOURNAL OF GEOPHYSICAL RESEARCH, VOL. 106, NO. A3, PAGES 3799–3810, MARCH 1, 2001

Collisionless reconnection supported by nongyrotropic pressure effects in hybrid and particle simulations

Masha M. Kuznetsova[1] and Michael Hesse
Electrodynamics Branch, NASA Goddard Space Flight Center, Greenbelt, Maryland

Dan Winske
Applied Theoretical Physics Division, Los Alamos National Laboratory, Los Alamos, New Mexico

Abstract.
This paper presents the detailed comparative analysis of full particle and hybrid simulations of collisionless magnetic reconnection. The comprehensive hybrid simulation code employed in this study incorporates essential electron kinetics in terms of the evolution of the full electron pressure tensor in addition to the full ion kinetics and electron bulk flow inertia effects. As was demonstrated in our previous publications, the electron nongyrotropic pressure effects play the dominant role in supporting the reconnection electric field in the immediate vicinity of the neutral X point. The simulation parameters are chosen to match those of the Geospace Environmental Modeling (GEM) "Reconnection Challenge." It is that these comprehensive hybrid simulations perfectly reproduce the results of full particle simulations in many details. Specifically, the time evolutions of the reconnected magnetic flux and the reconnection electric field, as well as spatial distributions of current density and magnetic field at all stages of the reconnection process, are found to be nearly identical for both simulations. Comparisons of variations of characteristic quantities along the x and z axes centered around the dominating X points also revealed a remarkable agreement. Noticeable differences are found only in electron temperature profiles, i.e., in the diagonal electron pressure tensor components. The deviation in the electron heating pattern in hybrid simulations from that observed in particle simulations, however, does not affect parameters essential for the reconnection process. In particular, the profiles of the off-diagonal components of the electron pressure tensor are found to be very similar for both runs and appear unaffected by heat flux effects. Both simulations also demonstrate that the E_y component of the electric field is nearly constant inside the diffusion region where ions are nonmagnetized. We demonstrate that the simple analytical estimate for the reconnection electric field as a convection electric field at the edge of the diffusion region very well reproduces the reconnection electric field observed in the simulations.

1. Introduction

Magnetic reconnection is widely believed to play an important role in a broad range of physical phenomena in space plasma involving fast release of magnetic energy. The key element of magnetic reconnection is violation of the frozen magnetic flux constraint $\mathbf{E}+\mathbf{v}\times\mathbf{B}=0$ in some localized regions of space (so-called "diffusion regions") [*Vasyliunas*, 1975]. A considerable amount of effort has been made to advance our understanding of the microphysics of the diffusion region in collisionless plasma [e.g., *Galeev et al.*, 1978; *Swift*, 1986; *Hoshino*, 1987; *Hewett et al.*, 1988; *Prittchet*, 1991; 1996; *Cai et al.*, 1994, *Pritchett and Büchner*, 1995; *Tanaka*, 1995; *Horiuchi and Sato*, 1994, 1997; *Biskamp et al.*, 1995; *Cai and Lee*, 1997; *Kuznetsova et al.*, 1998, 2000; *Shay et al.*, 1998; *Hesse and Winske*, 1998, *Hesse et al.*, 1999, this issue]. At the present time there is little doubt that kinetic effects play a significant role in collisionless magnetic reconnection and that particle distribution functions in diffusion region are essentially nongyrotropic. Deviation from gyrotropy in particle distribution function manifests itself in nongyrotropic pressure tensor with nonzero off-diagonal components.

[1]Raytheon ITSS Corporation, Lanham, Maryland.

Paper number 1999JA001003.
0148-0227/01/1999JA001003$09.00

The important role of the off-diagonal components of the electron pressure tensor in the diffusion region was first emphasized by *Vasyliunas* [1975] and later investigated by a number of authors [e.g., *Dungey*, 1988; *Lyons and Pridmore-Brown*, 1990, 1994; *Hesse and Winske*, 1993; *Cai et al.*, 1994; *Kuznetsova et al.*, 1998]. In the two-dimensional y-independent configuration, reconnection is driven by the y component of the electric field $\mathbf{E}$. Since the magnetic field is equal to zero at the neutral X line, only the electron bulk flow inertia term

$$E_y^{in} = -\frac{m_e}{e}\left(\frac{\partial v_{ey}}{\partial t} + v_{ez}\frac{\partial v_{ey}}{\partial z} + v_{ex}\frac{\partial v_{ey}}{\partial x}\right) \quad (1)$$

and the nongyrotropic pressure term

$$E_y^{ng} = -\frac{1}{n_e e}\left(\frac{\partial P_{\mathrm{exy}}}{\partial x} + \frac{\partial P_{\mathrm{eyz}}}{\partial z}\right) \quad (2)$$

can yield a nonvanishing contribution to the reconnection electric field E_y^r responsible for the breaking the frozen flux constraint $\mathbf{E} + \mathbf{v} \times \mathbf{B} = 0$. Here n_e and $\mathbf{v}_e$ are the electron number density and bulk flow velocity, respectively, and P_{exy} and P_{eyz} are off-diagonal components of the full electron pressure tensor $\underline{\mathbf{P}}_e$.

In order to incorporate electron kinetic nongyrotropic effects into the fluid description, *Hesse and Winske* [1993, 1994] suggested the utilization of the hierarchy of moments of the Vlasov equation. Without approximation, first and second moments of the Vlasov equation can be presented in the following form [*Gartenhaus*, 1964; *Hesse and Birn*, 1992; *Hesse et al.*, 1995]:

$$\mathbf{E} + \mathbf{v}_e \times \mathbf{B} = -\frac{\nabla \cdot \underline{\mathbf{P}}_e}{e n_e} - \frac{m_e}{e}\frac{d\mathbf{v}_e}{dt} \quad (3)$$

$$\frac{\partial \underline{\mathbf{P}}_e}{\partial t} = -\underline{\mathbf{D}} - \underline{\mathbf{C}} - \nabla \cdot \underline{\overline{\mathbf{Q}}}, \quad (4)$$

where

$$\underline{\mathbf{D}} = \left[\mathbf{v}_e \cdot \nabla \underline{\mathbf{P}}_e + \underline{\mathbf{P}}_e \nabla \cdot \mathbf{v}_e + \underline{\mathbf{P}}_e \cdot \nabla \mathbf{v}_e + (\underline{\mathbf{P}}_e \cdot \nabla \mathbf{v}_e)^T\right].$$

$$\underline{\mathbf{C}} = \frac{e}{m_e}\left[\underline{\mathbf{P}}_e \times \mathbf{B} + (\underline{\mathbf{P}}_e \times \mathbf{B})^T\right]$$

Here $\nabla \cdot \underline{\overline{\mathbf{Q}}}$ denotes the divergence of the generalized heat flux, and the superscript T denotes the transpose matrix. Conventional fluid descriptions of the electrons in Hall-MHD and hybrid models usually omit the last term in (3) related to the electron bulk flow inertia and substitute the scalar pressure P for the full electron pressure tensor $\underline{\mathbf{P}}_e$, where the former is commonly calculated using the simple adiabatic or isothermal equation of state. In other words, all terms that can provide collisionless dissipation are removed from (3) and replaced by an ad hoc resistive term. In their comprehensive hybrid approach, *Hesse and Winske* [1993, 1994] and *Hesse et al.* [1995] neglected the electron bulk flow inertia in (3) but kept the contribution from the nongyrotropic electron pressure. In order to decouple the evolution equation for the full pressure tensor $\underline{\mathbf{P}}_e$ from the higher moments of the Vlasov equation, the divergence of the heat flux in (4) was omitted. They confirmed that pressure anisotropy is developed in regions with small magnetic field and nongyrotropic pressure effects can self-consistently support the magnetic reconnection.

Kuznetsova et al. [1998] performed comprehensive hybrid simulations keeping the electron bulk flow inertia term in (3). It was demonstrated that kinetic quasi-viscous effects associated with nongyrotropic pressure dominate over the electron bulk flow inertia in controlling the magnitude of the reconnection electric field and the structure of the dissipation region around the neutral X line. This conclusion was later confirmed by full particle simulations performed by *Hesse and Winske* [1998]. The comprehensive hybrid simulation model was recently improved and modified [*Kuznetsova et al.*, 2000] in order to incorporate the most essential heat flux effect observed in particle simulations by *Hesse and Winske* [1998], the isotropization of the diagonal components of the electron pressure tensor. Both hybrid and particle simulations [*Kuznetsova et al.*, 1998, 2000; *Hesse and Winske*, 1998; *Hesse et al.*, 1999] demonstrated that the spatial scales of the dissipation region where the electron nongyrotropic effects are important are determined by the amplitudes of the electron meandering motions in the vicinity of the X point.

In the present study we present a detailed comparison of comprehensive hybrid simulations and full particle simulations of the same reconnection configuration with parameters defined by the Geospace Environmental Modeling (GEM) "Reconnection Challenge." The goals of this comparison are to test the validity of the comprehensive hybrid simulations, to understand mechanisms determining the reconnection rate, and to find ways to represent non-MHD effects in MHD models. We focus on testing the model for the evolution of pressure tensor components and the approximation for the heat flux effects. We demonstrate that excessive electron heating due to approximate treatment of heat flux effects in hybrid simulations does not affect the reconnection rate. We perform detailed comparative analysis of profiles of characteristic quantities (such as, electron and ion outflow velocities, components of the electron pressure tensor, number density, and electric field) in the vicinity of the reconnection site. We demonstrate that the reconnection electric field matches the convection electric field at the edge of the diffusion region outside of which both ion electron species are magnetized and an ideal MHD treatment is applicable. Simulation models and initial conditions are described in section 2. The results of comparison of comprehensive hybrid simulations and particle simulations and testing the simple analytical estimate for the reconnection electric field are presented in section 3. The summary and conclusions are in section 4.

2. Simulation Models and Initial Conditions

Two and a half dimensional comprehensive hybrid simulations performed in this study use the following

set of equations for the advance of the electromagnetic fields

$$\frac{\partial \hat{\mathbf{S}}}{\partial t} = \nabla \times \hat{\mathbf{E}}, \quad \hat{\mathbf{S}} = \mathbf{B} - \delta_e^2 \nabla^2 \mathbf{B} \tag{5}$$

$$\hat{\mathbf{E}} = -\mathbf{v}_e \times \mathbf{B} - \frac{\nabla \cdot \underline{\mathbf{P}}_e}{en} - \frac{m_e}{e}(\mathbf{v}_e \cdot \nabla)\mathbf{v}_e \tag{6}$$

$$\frac{\partial \underline{\mathbf{P}}_e}{\partial t} = -\underline{\mathbf{D}} - \underline{\mathbf{C}} - \tau_{is}^{-1}(\underline{\mathbf{P}}_e{}^{\mathrm{diag}} - P_0 \underline{\mathbf{1}}). \tag{7}$$

Here n is the number density of both ions and electrons, i.e., the quasineutrality is assumed, $\delta_e = c/\omega_{pe} = (c^2 \epsilon_0 m_e/ne^2)^{1/2}$ is a local electron inertia length, $\underline{\mathbf{1}}$ is the unity tensor, $P_0 = \mathrm{Tr}\underline{\mathbf{P}}_e/3$ is an average value of the diagonal components of the electron pressure tensor, τ_{is} is an isotropization timescale. The off-diagonal components of tensor $\underline{\mathbf{P}}_e{}^{\mathrm{diag}}$ are equal to zero; the diagonal components of tensor $\underline{\mathbf{P}}_e{}^{\mathrm{diag}}$ are equal to the diagonal components of tensor $\underline{\mathbf{P}}_e$. The last term in (7), which isotropizes the diagonal components of the electron pressure tensor, is introduced in order to incorporate the most probable effect of the heat flux. Expressions for the cyclotron and driver tensors $\underline{\mathbf{C}}$ and $\underline{\mathbf{D}}$ are given in (4). For the results discussed below we have chosen $\tau_{is} = \Omega_{0i}^{-1}$, where $\Omega_{0i} = eB_0/m_i$ is the ion cyclotron frequency in the asymptotic magnetic field B_0. We found that results are not very sensitive to the value of τ_{is} as far as isotropization is fast enough to keep the diagonal terms of the same order of magnitude. In (5) it is taken into account that the number density and the ion current density variations are insignificant on the electron spatial scales.

The ion trajectories are followed on a rectilinear grid using a standard particle-in-cell method. The number density n and the ion bulk flow velocity $\mathbf{v}_i$ are calculated on the grid. The electron bulk flow velocity $\mathbf{v}_e$ is expressed through the ion bulk flow velocity $\mathbf{v}_i$ and the current density $\mathbf{j} = \nabla \times \mathbf{B}$. The generalized fields $\hat{\mathbf{S}}$ and $\hat{\mathbf{E}}$ are advanced in time using a predictor-corrector scheme [*Winske and Quest*, 1986], and the electromagnetic fields are calculated using standard numerical methods.

In order to test this version of the hybrid model we employ a recently developed 2 1/2 dimensional fully electromagnetic particle-in-cell code [*Hesse and Winske*, 1998; *Hesse et al.*, 1999]. The simulation scheme utilizes the Buneman layout and integrates the electromagnetic fields implicitly. Densities and fluxes are accumulated on the grid, on the basis of a rectangular particle shape function. Charge conservation is guaranteed by the iterative application of a Langdon-Marder-type [*Langdon*, 1992] correction to the electric field. The particle simulation scheme is explained in more details in the paper by *Hesse et al.* [this issue].

The problem of reconnection onset is beyond the scope of the present study. Here we focus on the nonlinear evolution of collisionless magnetic reconnection after the neutral X line has already formed. The initial configuration with a neutral X point is provided by a Harris one dimensional current sheet with a superposed small perturbation of the magnetic flux. The system dimensions and initial conditions follow the Geospace Environmental Modeling (GEM) "Reconnection Challenge." [*Drake et al.*, this issue]

$$\mathbf{B} = \frac{\partial A_y}{\partial z}\mathbf{e}_x - \frac{\partial \tilde{A}}{\partial x}\mathbf{e}_z \tag{8}$$

$$n = n_0 \exp(-2A_y/B_0 L) + n_b \tag{9}$$

$$A_y = A_{y0} + \tilde{A}$$

$$A_{y0} = -B_0 L \ln[\cosh(z/L)] \tag{10}$$

$$\tilde{A} = 0.1 B_0 \cos(2\pi x/L_x)\cos(\pi z/L_z).$$

Here L_x and L_z are the system dimensions, n_b is a uniform density background, $n_0 = B_0^2/2(T_i + T_e)$, and $n_0 \exp(-2A_y/B_0 L)$ is a perturbed number density proportional to the perturbed current density supporting the magnetic field configuration given in (8)

$$n_0 \exp(-2A_y/B_0 L) \approx (n_0 + \tilde{n}))\cosh^{-2}(z/L)$$

$$\tilde{n} \approx -(2n_0/B_0 L)\tilde{A}. \tag{11}$$

All physical quantities are normalized to combinations of the ion inertial length $\delta_{0i} = c/\omega_i = (c^2 \epsilon_0 m_i/n_0 e^2)^{1/2}$ defined with n_0 and the ion cyclotron frequency $\Omega_{0i} = eB_0/m_e$ defined with B_0. The half thickness of the current sheet L is adopted to be equal to $0.5\delta_{0i}$.

The system dimensions are $L_x \times L_z = 25.6\delta_{0i} \times 12.8\delta_{0i}$ with 400×200 cells in the system. For the ion/electron mass ratio $m_i/m_e = 25$ used in the simulations this corresponds to the spatial resolution no less than 4 grid points per the electron inertial length. The electron/ion temperature ratio is chosen as $T_e/T_i = 0.2$. A time step $dt = 0.008\Omega_{0i}^{-1}$ is used.

For the particle simulations two sets of electron and ion species are utilized: current-carrying population (4×10^6 ions and electrons each) and uniform plasma background (2×10^6 ions and electrons each). The background density is set to $n_b = 0.2n_0$ with the background temperatures identical to the current carrying species. For the hybrid simulations, only ions are initialized as particles, while electrons are initialized as an isotropic fluid. About 3×10^6 ions are initialized as a current-carrying population; another 1.5×10^6 ions are initialized as a uniform background. Periodical boundary conditions are assumed at the left ($x = 0$) and right ($x = 25.6\delta_{0i}$) boundaries for both particles and fields. At the top ($z = L_z/2 = 6.4\delta_{i0}$) and the bottom ($z = -L_z/2 = -6.4\delta_{i0}$) boundaries, ions are specularly reflected and $E_y = E_z = dE_x/dz = 0$.

3. Results

Plate 1 illustrates color-coded current density distributions with superimposed contour plots of magnetic flux at several stages of the magnetic reconnection ($t = 0$, 10, 15, 20) for the hybrid simulations. A similar set of plots for the particle simulations (also at $t = 0$, 10, 15, 20) is shown in the paper by *Hesse et al.* [this issue]. It can be seen that both set of plots are similar

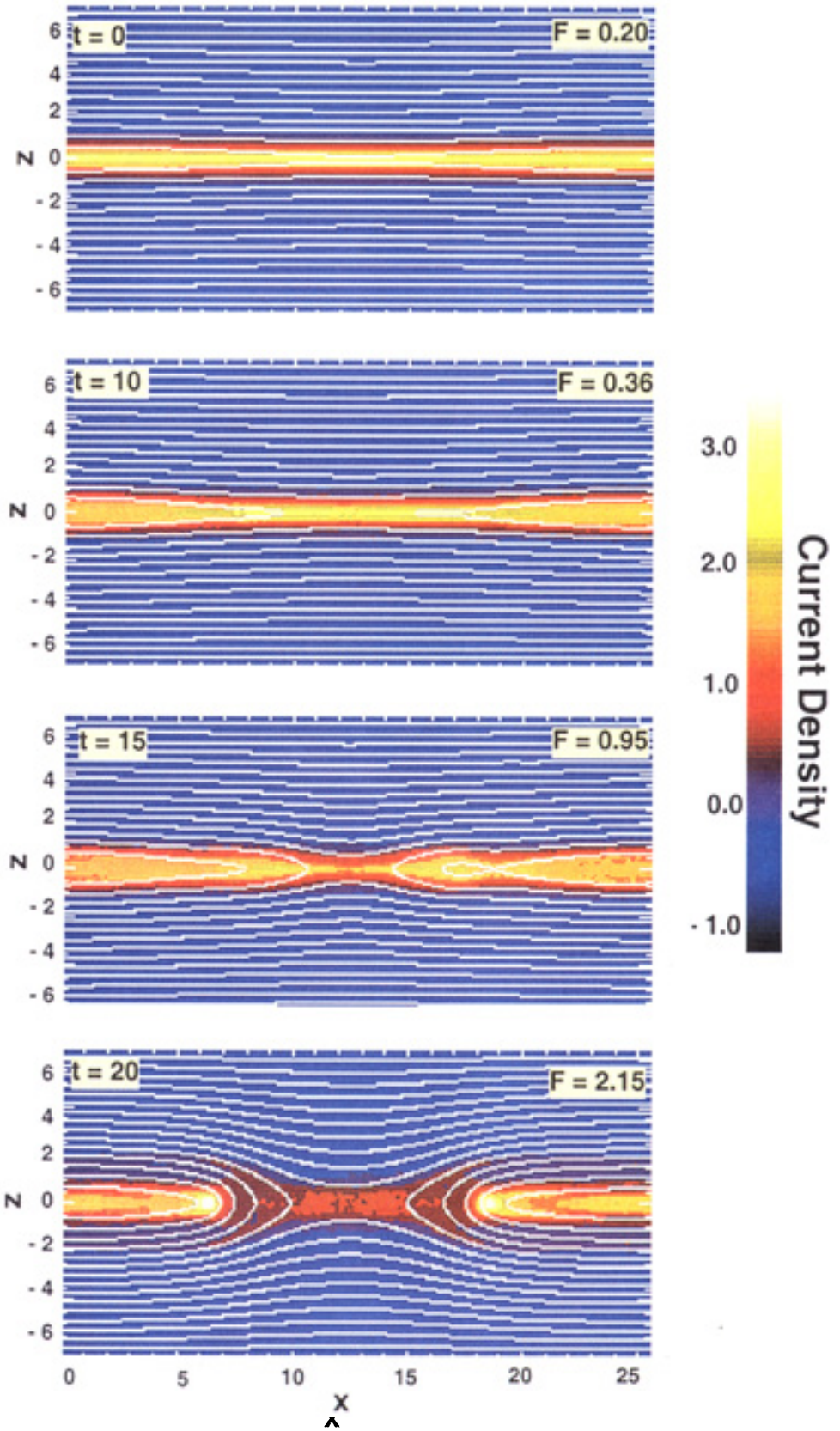

Plate 1. Magnetic field evolution and current density (color coded) evolution for the comprehensive hybrid simulations.

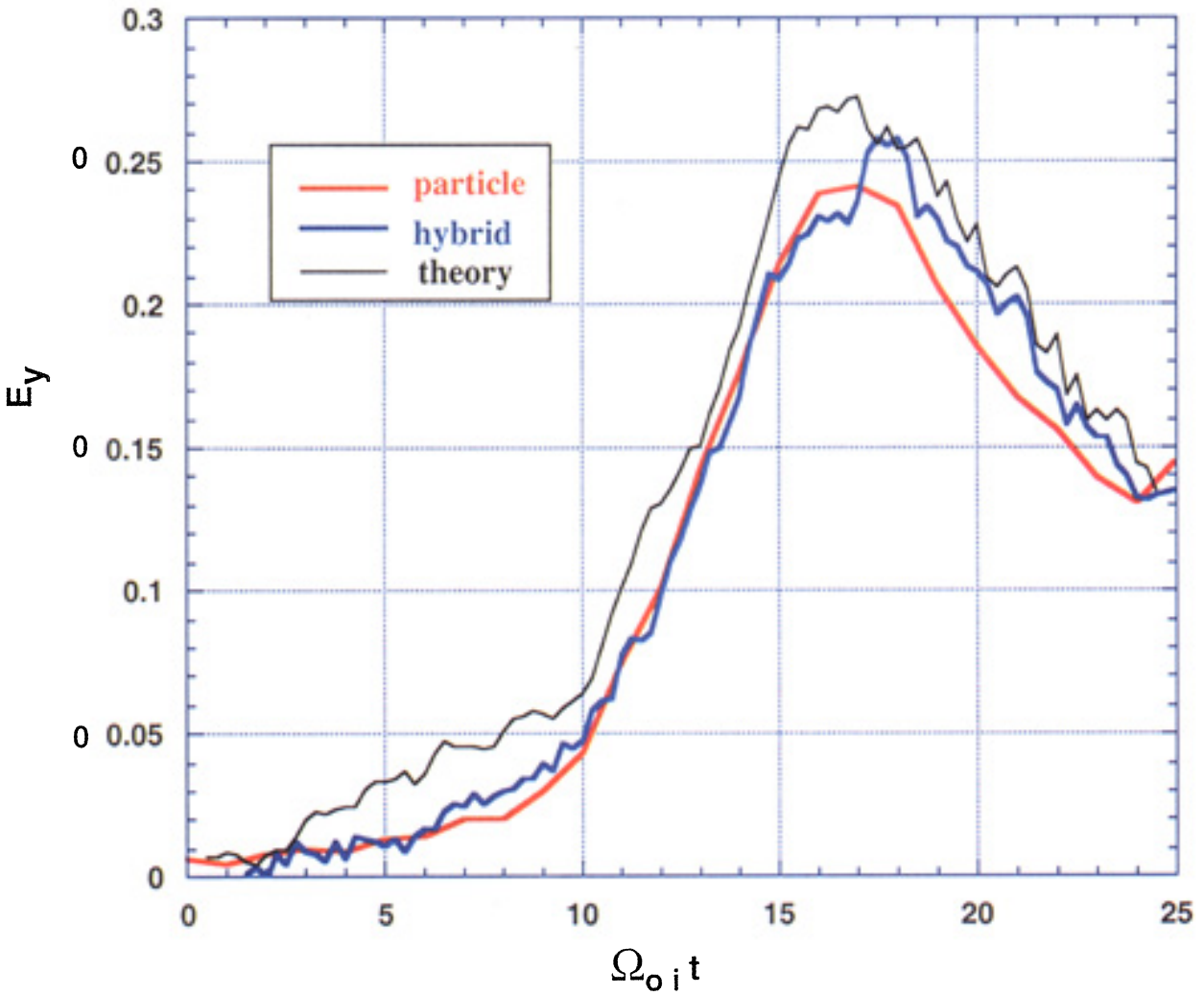

Plate 2. Time evolution of the reconnection electric field at the dominating X point for hybrid (blue curve) and particle (red curve) simulations. The black curve corresponds to the convection electric field at the edge of the diffusion region $v_x(d_{ix})B_z(d_{ix}) \approx (2m_iT_i/e^2)^{1/2}\partial v_x/\partial x$ independent of the electron mass or temperature.

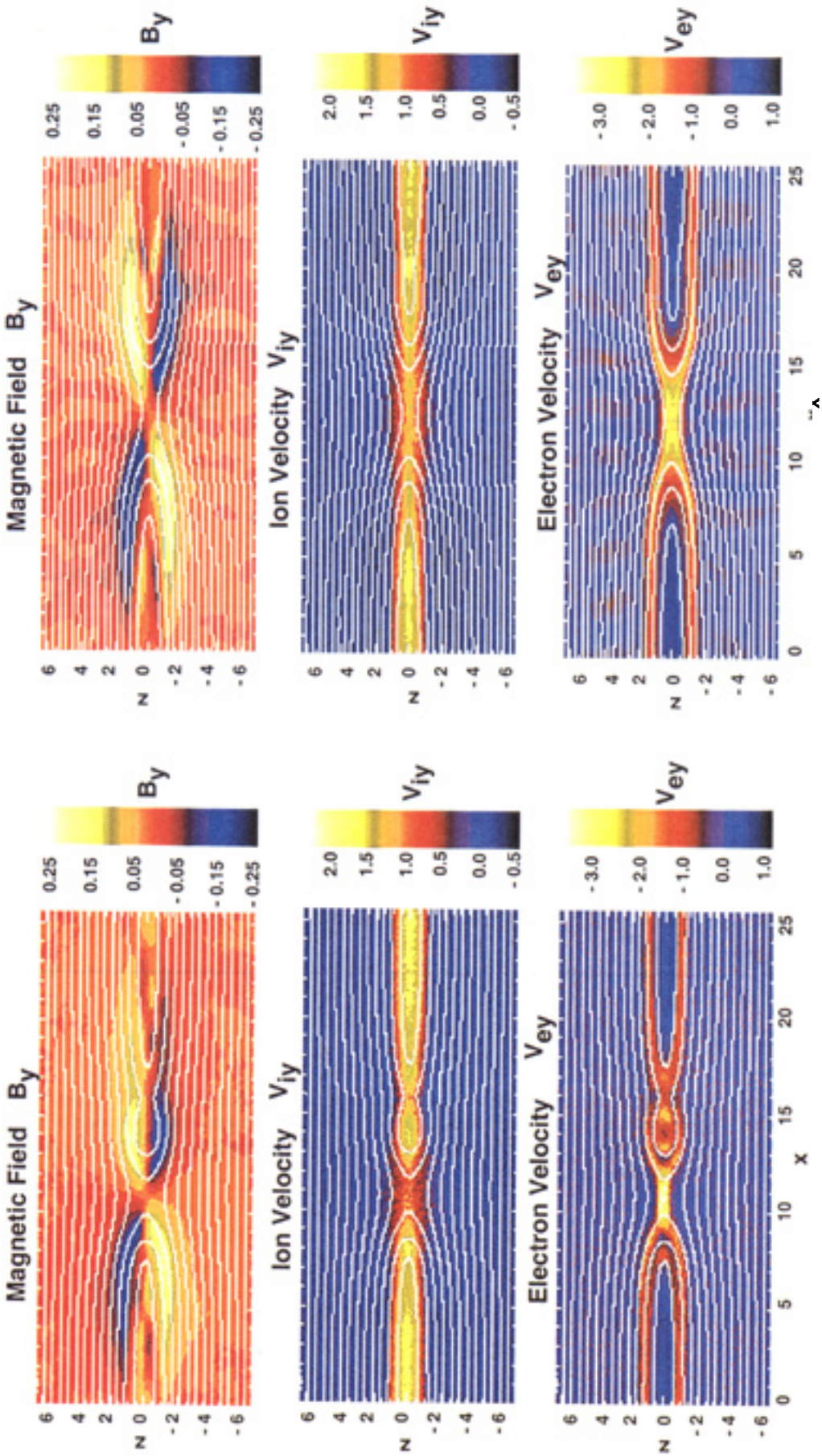

Plate 3. The color-coded y components of the magnetic field B_y and ion and electron bulk flow velocities v_{iy} and v_{ey} at $t = 17$ for the particle simulations.

Plate 4. The color-coded y components of the magnetic field B_y and ion and electron bulk flow velocities v_{iy} and v_{ey} at $t = 17$ for the hybrid simulations.

in many details with an exception of a small magnetic island created in the particle simulations as a results of splitting of the initial reconnection site. A much less developed small magnetic island can also be distinguished at $t = 15$ in hybrid simulations. The small magnetic island disappeares when one of the reconnection sites becomes dominant.

The earlier appearance of small magnetic island reflects a more noisy nature of particle simulations in comparison with hybrid simulations. For a slightly different initial reconnection geometry with larger initial magnetic perturbation or for magnetic configurations with larger initial thickness of the current sheet, the small magnetic island does not form [*Hesse and Winske*, 1998, 1999; *Kuznetsova et al.*, 2000]. Increasing the number of particle per cell in particle simulations can also reduce the size of the small magnetic island. The presence of the island does not affect the similarity of the plasma and field structure in the diffusion region. In particular, the current density gradient scales in the vicinity of the reconnection sites are nearly identical for both simulations at all stages of the reconnection process. For both simulations the areas of increased current density move away from the neural X line in the course of the reconnection growth, and the current density exhibits a saddle point at the reconnection site. Below we will disregard the small magnetic island and focus our attention on the structure of the dissipation region in the vicinity of the dominating X points.

Comparison of the overall system evolution for the particle and hybrid runs are illustrated in Figure 1 in terms of the time history of the reconnected magnetic flux $F(t)$ [see, *Hesse and Winske*, 1998, *Kuznetsova et al.*, 2000]. The solid curve corresponds to the hybrid simulations; the dashed curve corresponds to the particle simulations. The figure demonstrates that with an exception of a small time shift for times larger than $t = 20$, the evolution of the reconnected magnetic flux is essentially the same for both runs. The temporal evolution of the reconnection electric field at the X point which is proportional to the reconnection rate dF/dt is displayed in Plate 2. The red curve corresponds to the particle simulations; the blue curve corresponds to the hybrid simulations. For the particle simulations the electric field at the most advance X point is shown. The black curve corresponds to a simple analytical estimate for the reconnection electric field as a convection electric field at the edge of the diffusion region $d_{ix} \times d_{iz}$,

$$d_{ix} = (m_i T_i / e^2 B'^2_z)^{1/4},\ d_{iz} = (m_i T_i / e^2 B'^2_x)^{1/4}, \quad (12)$$

where ions are nongyrotropic (i.e., unmagnetized)

$$E_y^{\rm rec} \approx v_x(d_{ix}) B_z(d_{ix}) \approx \frac{1}{e}\sqrt{2 m_i T_i}\frac{\partial v_x}{\partial x}. \quad (13)$$

Here the continuity of flow is assumed, and the x component of the plasma bulk flow velocity and the z component of the magnetic field at the edge of the diffusion region are estimated as $v_x \approx v'_x d_{ix}$ and $B_z \approx B'_z d_{ix}$, respectively. Outside of the diffusion region $|x| > d_{ix}$, $|z| > d_{iz}$, both ion and electron species are magnetized, the one fluid MHD approach is applicable and the frozen magnetic flux constraint $\mathbf{E} + \mathbf{v} \times \mathbf{B} = 0$ is valid.

The spatial scales of the diffusion region and partial derivative of the plasma bulk flow velocity v_x in the vicinity of the reconnection site $x = x_0$, $z = 0$ averaged over the diffusion region are taken from the comprehensive hybrid simulations. Variations in the ion temperature are neglected, i.e., for normalization adopted in this study $T_i \approx 0.42$. It is also taken into account that the plasma bulk flow velocity v_x is almost identical to the ion flow velocity, i.e., $v_x \approx v_{ix}$.

An excellent agreement between particle and hybrid simulations and an analytical estimate can be observed. The fast growth starts at about $t = 10$ when the current density is strongly concentrated in the vicinity of the reconnection site (see Plate 1). All curves reach their maxima of the order of $0.25 B_0 v_A$ between $t = 17$ and $t = 18$. After that the compression of the magnetic field due to the finite size of the magnetic island in the periodical system decreases the gradient of the outflow velocity $\partial v_x/\partial x$ and slows down the reconnection.

Similarly to the previous results by *Kuznetsova et al.* [1998] and *Hesse and Winske* [1998] for both hybrid and particle simulations, the reconnection electric field is supported primarily by kinetic nongyrotropic pressure effects. The contribution from the electron bulk flow inertia is negligibly small. The analytical estimate given in (13) very well reproduces the reconnection electric field. The important point there is that the expression (13) is independent of electron mass and temperature. This result matches the conclusion made in the paper by *Hesse et al.* [1999] where the dependence on the electron mass was investigated. This is also consistent with conclusion made earlier by *Galeev et al.* [1978] and *Biskamp et al.* [1995] that the neutral X point reconnection rate is controlled exclusively by the ions.

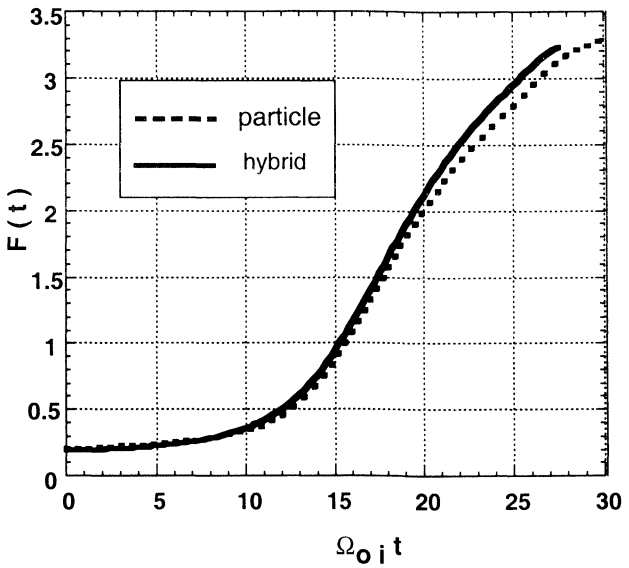

Figure 1. Time history of the reconnected magnetic flux for the particle (dashed curve) and comprehensive hybrid (solid curve) simulations.

For further comparison we choose the time $t = 17$ when the reconnection rate is close to its maximum for both hybrid and particle runs, and the level of reconnected flux F is close to 1.5. The spatial scale of the diffusion region d_{ix} at this time is ~ 2.5. The color-coded y components of the magnetic field B_y and ion and electron bulk flow velocities v_{iy} and v_{ey} are shown in Plates 3 and 4 for particle and hybrid simulation respectively. The quadrupolar structure of B_y is quite similar for both simulations. Similar quadropolar magnetic fields have also been observed in a number of previous studies [e.g., *Hesse and Winske*, 1994]. The distributions of the ion bulk flow velocity in the y direction are also very similar. In particular, it is seen that ions with a larger y component of the velocity are ejected out of the diffusion region. Both hybrid and particle simulations show that ion bulk flow velocity spatial distribution is much less modulated than the electron bulk flow velocity spatial distribution and that ion contribution to the current density in the diffusion region is small in comparison with the contribution from electrons. Gradient scales of the ion bulk flow velocity across the current sheet are of the order of the initial current sheet thickness and are quite similar for hybrid and particle runs.

The electron current velocity is concentrated around the X point in the region where electrons are nonmagnetized (i.e., nongyrotropic) with the spatial scales d_{ez}, d_{ex} of the order of the amplitude of the electron meandering motion in the quadrupole magnetic configuration [*Laval et al.*, 1966; *Dobrowolny*, 1968; *Galeev et al.*, 1978; *Kuznetsova et al.*, 1998, 2000; *Hesse et al.*, 1999, this issue]

$$d_{ex} = (m_e\hat{T}_e/e^2B'^2_z)^{1/4},\ d_{ez} = (m_e\hat{T}_e/e^2B'^2_x)^{1/4}, \quad (14)$$

where $\hat{T}_e$ is an average electron temperature in the diffusion region, $B'_z = \partial B_z(x,0)/\partial x$, $B'_x = \partial B_x(0,z)/\partial z$. The electron nongyrotropic region is

$$\alpha_{ei} = (m_e\hat{T}_e/m_i\hat{T}_i)^{1/4}$$

times smaller than the diffusion region (i.e., the ion nongyrotropic region). For the temperature ratio $T_e/T_i = 0.2$ and the mass ratio $m_e/m_i = 1/25$, the factor α_{ei} is $\sim 1/3$; for the realistic mass ratio it is 10 times smaller. By careful comparison of the distributions of the electron current velocity for particle and hybrid simulations, it can be noticed that the electron current sheet is slightly thinner for the particle case than for the hybrid case. The difference in the electron spatial scale is likely to be associated with the difference in the electron temperature. It is reasonable to assume that the evolution equation for the diagonal component of the pressure tensor with neglected heat flux term employed in hybrid simulations can provide an excessive electron heating different from what is observed in particle simulations.

We now compare the variations of characteristic quantities along the x and z axes of the simulation domain. The plots are centered around the dominating X points.

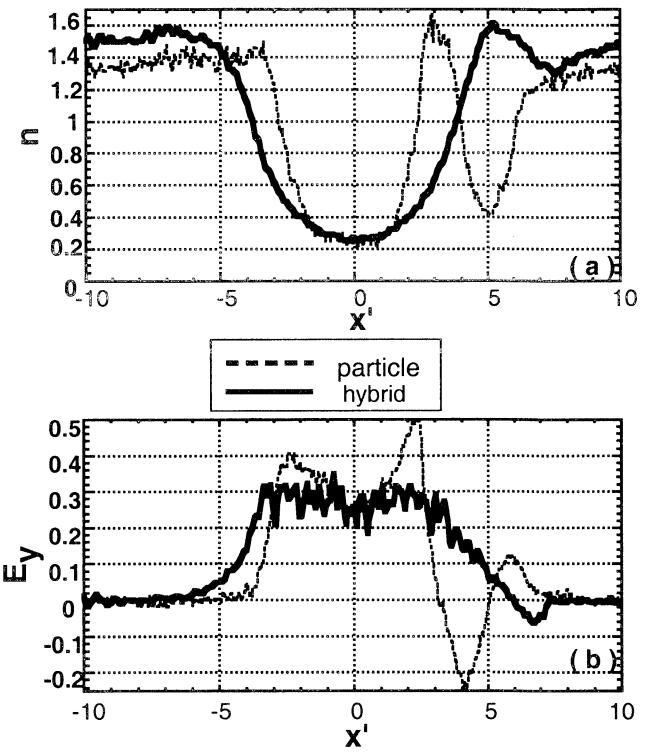

Figure 2. Comparison along the $x' = x - x_0$ axis of (a) number density and (b) E_y component of the electric field at $t = 17$ for particle (dashed curves) and hybrid (solid curves) simulations. The plots are centered around the dominating X points $x = x_0$, $z = 0$.

At $t = 17$ the dominating X point for the particle is located at $z = 0$, $x = x_0 \approx 10.9$, while for the hybrid simulations it is located at $z = 0$, $x = x_0 \approx 12.5$. Figures 2a and 2b show the dependence of the number density and E_y electric field component on $x' = x - x_0$. It is seen that densities and electric fields shown by solid black curves for hybrid simulations and by dashed curves for particle simulations are nearly identical inside the diffusion region $|x'| \ll 2.5$. The dependence of the diagonal components of the electron pressure tensor P_{xx}, P_{yy}, and P_{zz} on $x' = x - x_0$ for particle (dashed curves) and hybrid (solid curves) is shown in Figure 3. The excessive heating of electrons in hybrid simulations that already has been suspected while examining electron current velocity plots in Plates 3 and 4 is clearly seen in Figure 3. From results shown in Figure 2b and Figure 3 it can be estimated that

$$\hat{T}_e^{\rm hyb} \approx 0.4, \quad \hat{T}_e^{\rm part} \approx 0.16. \quad (15)$$

The ratio between the average temperatures in the vicinity of the X lines in hybrid and particle simulations $\tau_{\rm part}^{\rm hyb} = \hat{T}_e^{\rm hyb}/\hat{T}_e^{\rm part}$ is ~ 2.5, which corresponds to

$$\frac{d_{ez}^{\rm hyb}}{d_{ez}^{\rm part}} = \left(\frac{\hat{T}_e^{\rm hyb}}{\hat{T}_e^{\rm part}}\right)^{1/4} = \left(\tau_{\rm part}^{\rm hyb}\right)^{1/4} \approx 1.3; \quad (16)$$

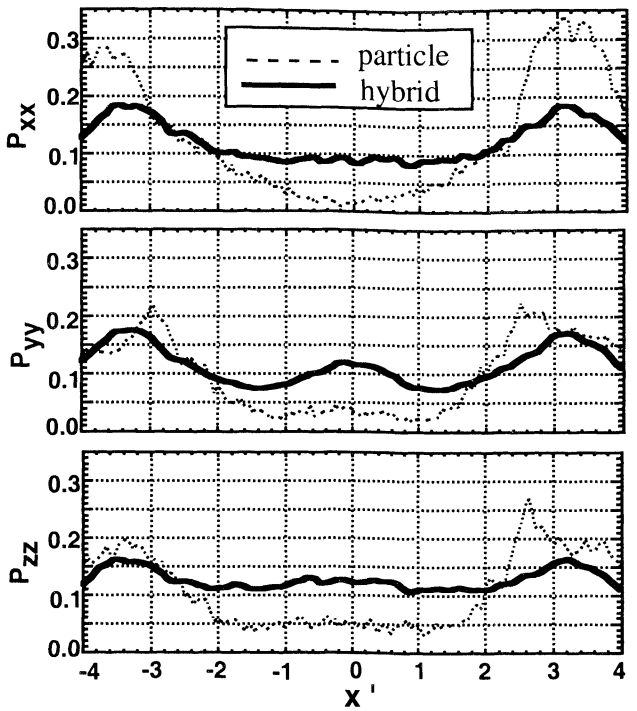

Figure 3. Comparison along the $x' = x - x_0$ axis of diagonal components of the electron pressure tensor at $t = 17$ for particle (dashed curves) and hybrid (solid curves) simulations. The plots are centered around the dominating X points..

that is, the excessive electron heating in hybrid simulations results in slightly thicker electron gradient scales, which have already been noticed in Plate 4. Therefore the model for the electron heating (evolution of the diagonal components of the electron pressure tensor) can be refined in the future. However, the similarities in the overall system evolution in hybrid and particle simulations illustrated in Plates 1 and 2 and Figure 1 [see also *Hesse et al.*, this issue] as well as similarities in structures of the reconnection electric fields E_y shown in Figure 2b indicate that the deviation in the electron heating pattern in hybrid simulations from that observed in particle simulations does not affect parameters essential for the reconnection process.

Indeed, it was demonstrated by *Kuznetsova et al.* [1998, 2000] and by *Hesse and Winske* [1998] and confirmed in simulations discussed above in this section that the dominating contribution to the reconnection electric field comes from the nongyrotropic pressure term given in (2); that is, the reconnection electric field is controlled by partial derivatives of the off-diagonal components of the electron pressure tensor $\partial P_{exy}/\partial x$ and $\partial P_{eyz}/\partial z$. Figure 4a shows variations of P_{exy} along $x' = x - x_0$ for $z = 0$, and Figure 4b shows variations of P_{eyz} along z for $x = x_0$ at $t = 17$ within the diffusion region around the X point ($x = x_0$, $z = 0$) for particle ($x_0 \approx 10.9$) and hybrid ($x_0 \approx 12.5$) simulations. For the hybrid simulations the off-diagonal components are found from the solution of the reduced second moment of the Vlasov equation, while for the particle simulations those are calculated using the electron distribution function.

Although the graphs of the particle model results appear more oscillatory, the average behavior is strikingly similar. Despite that the dashed plots corresponding to particle simulations, are more oscillating than solid plots corresponding to hybrid simulations the striking similarities in averaged behavior of plots are apparent. In particular, P_{exy} and P_{eyz} reach their maxima close to the edges of the electron nongyrotropic region. Within the electron nongyrotropic region the averaged slopes (i.e., derivatives) are virtually the same for both simulations. It also can be noticed that $\partial P_{eyz}/\partial z$ is approximately equal to $\partial P_{exy}/\partial x$ for both simulations which is consistent with simple analytical estimates presented by *Hesse et al.* [1999] and *Kuznetsova et al.* [2000]. This analysis confirmed the validity of the model for the evolution of the off-diagonal electron pressure tensor components employed in the comprehensive hybrid simulations which very well reproduce the results of particle simulations. Heat flux effects modify only the evo-

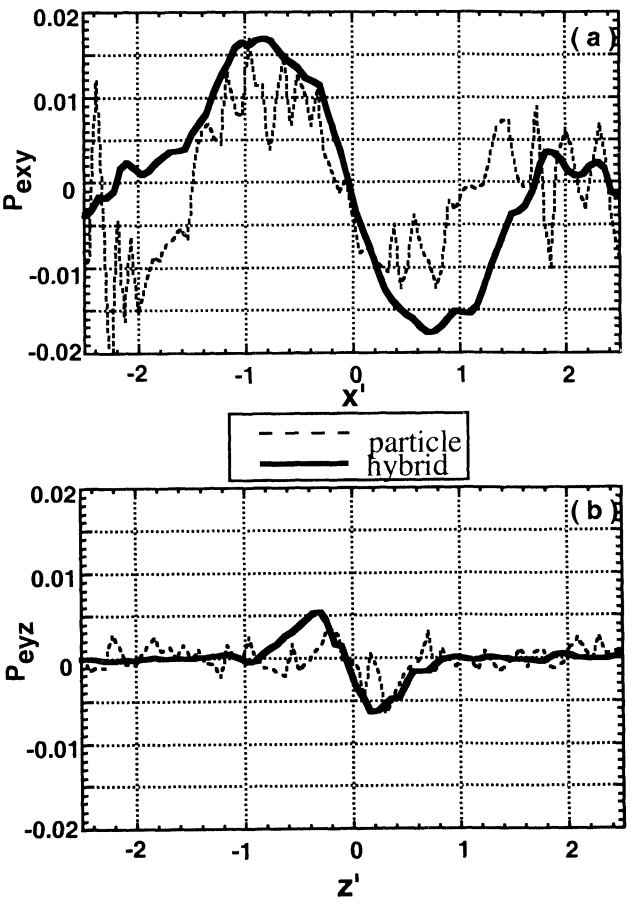

Figure 4. (a) Comparison along the $x' = x - x_0$ axis of P_{exy} component of the electron pressure tensor at $t = 17$ for particle (dashed curves) and hybrid (solid curves) simulations; (b) Comparison along the z axis of P_{eyz} component of the electron pressure tensor at $t = 17$ for particle (dashed curves) and hybrid (solid curves) simulations. The plots are centered around the dominating X points.

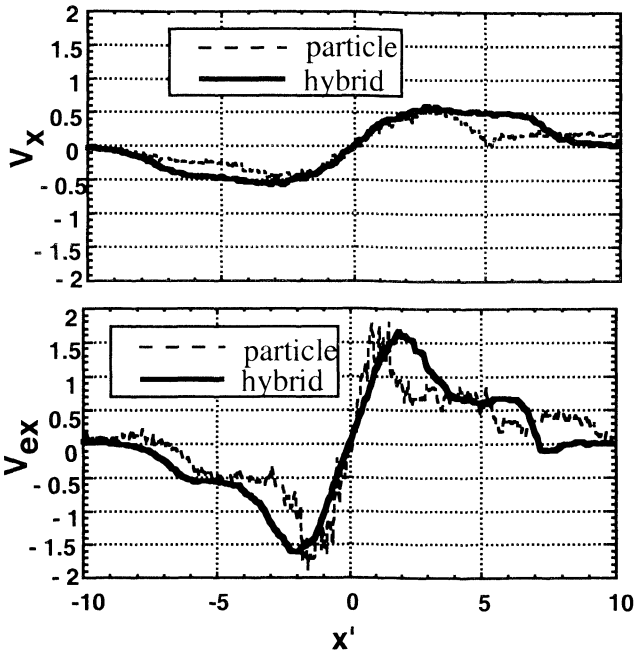

Figure 5. Comparison along the $x' = x - x_0$ axis of ion and electron bulk flow velocity components v_x and v_{ex} at $t = 17$ for particle (dashed curves) and hybrid (solid curves) simulations.

lution of the diagonal components of the pressure tensor but are not reflected as much in the off-diagonal components and consequently in the reconnection electric field. Therefore the comprehensive hybrid model incorporates the most essential electron kinetic effects for the reconnection process.

The comparative analysis of hybrid and particle simulations continues in Figures 5 and 6, where variations of ion and electron bulk flow velocity components v_x and v_{ex} along $x' = x - x_0$ axis and v_z and v_{ez} along z axis are plotted. It can be seen that the ion bulk flow velocity profiles shown in Figures 5a and 5b are very similar. According to the simple formula (13), the similarity of ion bulk flow velocity profiles $\partial v_x/\partial x$ in hybrid and particle simulations should give rise to similar reconnection electric fields which is consistent with the results illustrated in Plate 2 and Figure 2b. At the first glance the electron flow velocity profiles shown in Figures 5b and 6b also appear to be quite close. Both simulations give $\partial v_{ex}/\partial x \approx -\partial v_{ez}/\partial z$ which is consistent with the assumption made by *Kuznetsova et al.* [2000] and *Hesse et al.* [1999] where the following estimate for the electric field inside the electron nongyrotropic region was derived

$$E^{\rm rec} \approx \frac{1}{e}\sqrt{2m_e\hat{T}_e}\frac{\partial v_{ex}}{\partial x}. \qquad (17)$$

However, after more detailed examining of plots shown in Figure 5b, one can notice that the slope of the electron flow velocity profile inside the electron nongyrotropic region appears to be more steep for the particle simulations than for the hybrid simulations. Indeed,

$$\left(\frac{\partial v_{ex}}{\partial x}\right)^{\rm hyb} \approx 1.1, \quad \left(\frac{\partial v_{ex}}{\partial x}\right)^{\rm part} \approx 1.73. \qquad (18)$$

From the estimates presented in (15) and (18), one can see that the difference in gradients of the electron flow velocity v_{ex} in hybrid and particle simulations almost exactly "compensates" the difference in the electron temperature and according to (17) gives rise to almost identical electric fields, i.e.,

$$\sqrt{\hat{T}_e^{\rm hyb}}\left(\frac{\partial v_{ex}}{\partial x}\right)^{\rm hyb} \approx \sqrt{\hat{T}_e^{\rm part}}\left(\frac{\partial v_{ex}}{\partial x}\right)^{\rm part}. \qquad (19)$$

Similar "adjustments" of the electron outflow velocity gradient $\partial v_{ex}/\partial x \sim m_e^{-1/2}$ were observed in particle simulations with varying electron mass [*Hesse et al.*, 1999].

One can easily check that the electron nongyrotropic contribution to the electric field given in (17) perfectly matches the reconnection electric field (13) which is equal to the convection electric field $v_x B_z$ at the edge of the diffusion region [*Kuznetsova et al.*, 2000]

$$\sqrt{2m_e\hat{T}_e}\frac{\partial v_{ex}}{\partial x} \approx \sqrt{2m_i T_i}\frac{\partial v_x}{\partial x}. \qquad (20)$$

Therefore, by adjusting the outflow velocity profile, electrons can provide just the necessary nongyrotropic pressure to support any electric field imposed by the overall system evolution controlled by the ions.

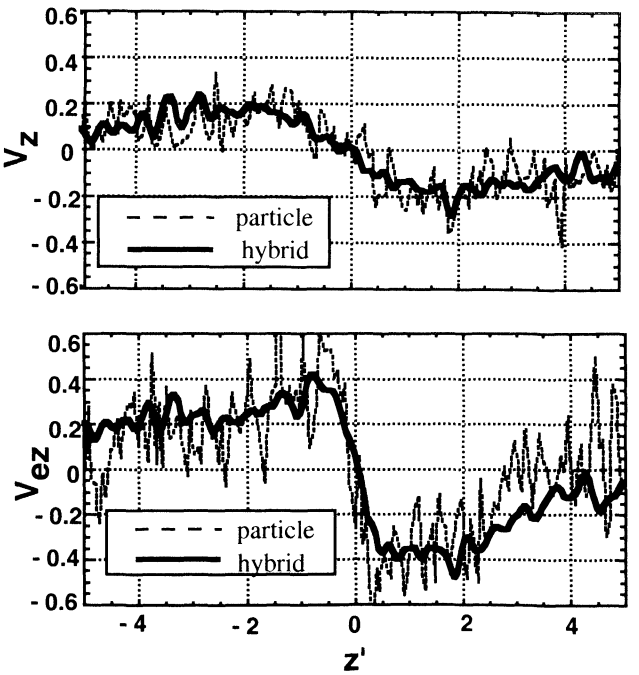

Figure 6. Comparison along the z axis of ion and electron bulk flow velocity components v_z and v_{ez} at $t = 17$ for particle (dashed curves) and hybrid (solid curves) simulations.

4. Summary and Conclusions

In this paper we presented a detailed comparative analysis of full particle and hybrid simulations of collisionless magnetic reconnection. The hybrid code employed in this study incorporates thermal electron inertia effects on top of electron bulk flow inertia and full ion kinetic treatment. The simulation parameters were chosen to match those of the "Reconnection Challenge," defined by a modeling working group within the Geospace Environment Modeling (GEM) program of the National Science Foundation. The aim of this program was to compare different simulations of the same reconnection configurations with the goal of understanding the physics underlying the reconnection process, as well as finding ways to represent the most essential microphysics in some reduced form in large-scale models.

The comparative analysis of the results of the comprehensive hybrid simulations and the full particle simulations with similar setups revealed an excellent quantitative agreement. Time evolution of the reconnected magnetic flux and the reconnection electric field, as well as spatial distribution of current density and magnetic field at all stages of the reconnection process were found to be nearly identical for both simulations. Similarly to the previous results by *Kuznetsova et al.* [1998] and *Hesse and Winske* [1998] for both hybrid and particle simulations, the dominant contribution to the reconnection electric field at the neutral X point results from the electron nongyrotropic pressure term depending on the spatial derivatives of the off-diagonal components of the electron pressure tensor (see (2)). The contribution from the electron bulk flow inertia is negligibly small.

More detailed comparisons of variations of characteristic quantities along the x and z axes of the simulation domain were performed for time $t = 17$ when the reconnection electric field is close to its maximum for both simulations. A comparison of the diagonal components of the electron pressure tensor revealed excessive electron heating in the hybrid simulations in comparison with the particle simulations.

The deviation in the electron heating pattern in hybrid simulations, however, did not affect parameters essential for the reconnection process. In particular, the profiles of the off-diagonal components of the electron pressure tensor were found to be very similar for both runs and appear not affected by the heat flux effects. It also was demonstrated that the gradients of the electron flow velocity in the vicinity of the neutral X point $\partial v_{ex}/\partial x$ scale like $\hat{T}_e^{-1/2}$. That is, the electron flow velocity profile in hybrid simulations self-consistently adjusts to "compensate" for the error in the electron temperature, owing to an approximate description of the electron heat flux effects, and provides a nongyrotropic contribution to the electric field proportional to $\sqrt{\hat{T}_e}(\partial v_{ex}/\partial x)$ identical to that observed in particle simulations. Thus this study confirmed the validity of the model for the evolution of the off-diagonal electron pressure tensor components employed in the comprehensive hybrid simulations, which very well reproduce the results of particle simulations.

We further illustrated that the ion bulk flow velocity profiles are almost identical for both runs. The number densities within the diffusion region were also almost equal. This is not surprising since ions in both simulations were treated in a similar way. Both simulations also demonstrated that the E_y component of the electric field is nearly constant inside the diffusion region where ions are nonmagnetized.

We also showed that the simple analytical estimate for the reconnection electric field as a convection electric field at the edge of the diffusion region $E^{\rm rec} \approx v_x(d_{ix})B_z(d_{ix}) \approx (2m_iT_i/e^2)^{1/2}\partial v_x/\partial x$ very well reproduces the reconnection electric field seen in the simulations. This is a very good indication that this simple formula can be utilized by MHD models for treatment of regions of weak magnetic field in vicinities of neutral X points, where ions become unmagnetized (nongyrotropic). By introducing m_i and e as parameters, all quantities in expressions (12) and (13) for the spatial scales of the diffusion region and the reconnection electric field can be calculated within the framework of the MHD approach.

A matter of principle importance here is that the convection electric field at the edge of the diffusion region (i.e., the reconnection electric field) is independent of electron mass and temperature. It was demonstrated that electron nongyrotropic contribution to the electric field matches the convection electric field at the edge of the diffusion region. Therefore, by adjusting the outflow velocity profile, electrons can provide just the necessary nongyrotropic pressure to support any electric field imposed by the overall system evolution controlled by the ions. This result matches the conclusion made by *Hesse et al.* [1999] where the dependence on the electron mass was investigated [see also *Hesse et al.*, this issue]. This is also consistent with the conclusion made earlier by *Galeev et al.* [1978] and *Biskamp et al.* [1995] that the neutral X point reconnection rate is controlled by the large-scale dynamics.

Acknowledgments. We appreciate stimulating and helpful discussions with J. Birn, K. Schindler, J.F. Drake, and M. Shay. This work was supported by the NASA SR&T and SECTP Programs.

Janet G. Luhmann thanks Dieter Biskamp and another referee for their assistance in evaluating this paper.

References

Biskamp, D., E. Schwarz, and J.F. Drake, Ion-controlled collisionless magnetic reconnection, *Phys. Rev. Lett., 75*, 3850, 1995.

Cai, H.J., and L.C. Lee, The generalized Ohm's law in collisionless magnetic reconnection, *Phys. Plasmas, 4*, 509, 1997.

Cai, H.J., D.Q. Ding, and L.C. Lee, Momentum transport near a magnetic X line in collisionless reconnection, *J. Geophys. Res., 99*, 35, 1994.

Coppi, B., G. Laval, and R. Pellat, Dynamics of the geomagnetic tail, *Phys. Rev. Lett., 16*, 1207, 1966.

Dungey, J. W., Noise-free neutral sheets, in *Reconnection in*

Space Plasma, edited by T. D. Guyenne and J. J. Hunt, *Eur. Space Agency Spec. Publ., ESA SP-285*, 15, 1988.

Dobrowolny, M., Instability of a neutral sheet, *Nuovo Cimento, 55*, 427, 1968.

Hesse, M., and J. Birn, Three-dimensional MHD modeling of magnetotail dynamics for different polytropic indices, *J. Geophys. Res., 97*, 3965, 1992.

Hesse, M., and D. Winske, Hybrid simulations of collisionless ion tearing, *Geophys. Res. Lett., 20*, 1207, 1993.

Hesse, M., and D. Winske, Hybrid simulations of collisionless reconnection in current sheets, *J. Geophys. Res., 99*, 11,177, 1994.

Hesse, M., and D. Winske, Electron dissipation in collisionless magnetic reconnection, *J. Geophys. Res., 103*, 26,479, 1998.

Hesse, M., D. Winske, and M. Kuznetsova, Hybrid modeling of collisionless reconnection in two-dimensional current sheets: Simulations, *J. Geophys. Res., 100*, 21,815, 1995.

Hesse, M., K. Schindler, J. Birn, and M. Kuznetsova, The diffusion region in collisionless magnetic reconnection, *Phys. Plasmas, 6*, 1781, 1999.

Hesse, M., J. Birn, and M. Kuznetsova, Collisionless magnetic reconnection: Electron processes and transport modeling, submitted to *J. Geophys. Res.*, this issue.

Hewett, D. W., G. E. Francis, and C. E. Max, New regimes of magnetic reconnection in collisionless plasmas, *Phys. Rev. Lett., 61*, 893, 1988.

Horiuchi, R., and T. Sato, Particle simulation study of driven magnetic reconnection in collisionless plasma, *Phys. Plasmas, 1*, 3587, 1994.

Horiuchi, R., and T. Sato, Particle simulation study of collisionless driven reconnection in a sheared magnetic field, *Phys. Plasmas, 4*, 277, 1997.

Hoshino, M., The electrostatic effect for the collisionless tearing mode, *J. Geophys. Res., 92*, 7368, 1987.

Galeev, A.A., F.V. Coroniti, and M. Ashour-Abdalla, Explosive tearing mode reconnection in the magnetospheric tail, *Geophys. Res. Lett., 5*, 707, 1978.

Gartenhaus, S., *Elements of Plasma Physics*, Holt, Rinehart, and Winston, Fort Worth, Tex., 1964.

Kuznetsova M.M., M. Hesse, and D. Winske, Kinetic quasi-viscous and bulk flow inertia effects in collisionless magnetotail reconnection, *J. Geophys. Res., 103*, 199, 1998.

Kuznetsova M.M., M. Hesse, and D. Winske, Toward a transport model of collisionless magnetic reconnection, *J. Geophys. Res., 105*, 7601, 2000.

Langdon, A.B., On enforcing Gauss' law in electromagnetic particle-in-cell cedes, *Comp. Phys. Comm., 70*, 447, 1992.

Laval, G., R. Pellat, and M. Vullemin, Instabilities electromagnetiques des plasmas sans collisions, in *Plasma Physics and Controlled Neuclear Fusion Research*, vol. 2, pp. 259-263, Int. Atomic Energy Agency, Vienna, 1966.

Lyons, L. R., and D. C. Pridmore-Brown, Force balance near an X line in a collisionless plasma, *J. Geophys. Res., 95*, 20,903, 1990.

Lyons, L. R., and D. C. Pridmore-Brown, Particle acceleration very near an X line in a collisionless plasma, in *Space Plasmas: Coupling Between Small and Medium Scale Processes, Geophys. Monogr. Ser.*, vol. 86, pp. 163-170, edited by M. Ashour-Abdalla and T. Chang, AGU, Washington, D.C., 1995.

Pritchett, P.L., and J. Büchner, Collisionless reconnection in configurations with a minimum in the equatorial magnetic field and with magnetic shear, *J. Geophys. Res., 100*, 3601, 1995.

Pritchett, P. L., F. V. Coroniti, R. Pellat, and H. Karimabadi, Collisionless reconnection in two-dimensional magnetotail equilibria, *J. Geophys. Res., 96*, 11,523, 1991.

Pritchett, P.L., F.V. Coroniti, and V. K. Decyk, Three-dimensional stability of thin quasi-neutral current sheets, *J. Geophys. Res., 101*, 27,413, 1996.

Shay, M.A., J.F. Drake, R.E. Denton, and D. Biskamp, Structure of the dissipation region during collisionless magnetic reconnection, *J. Geophys. Res., 103*, 9165, 1998.

Swift, D. W., Numerical simulations of tearing mode instabilities, *J. Geophys. Res., 91*, 219, 1986.

Tanaka, M., Macro-particle simulations of collisionless magnetic reconnection, *Phys. Plasmas, 2*, 2920, 1995.

Vasyliunas, V. M., Theoretical models of magnetic field line merging, 1, *Rev. Geophys., 13*, 303, 1975.

Winske, D., and K. B. Quest, Electromagnetic ion beam instabilities: Comparison of one- and two-dimensional simulations, *J. Geophys. Res., 91*, 8789, 1986.

M. Hesse and M. M. Kuznetsova, NASA Goddard Space Flight Center, Electrodynamics Branch, Greenbelt, MD 20771. (e-mail: masha@elbrus.gsfc.nasa.gov; hesse@gsfc.nasa.gov)

D. Winske, Los Alamos National Laboratory, Applied Theoretical Physics Division, Los Alamos, NM 87545. (e-mail: winske@lanl.gov)

(Received August 6, 1999; revised January 25, 2000; accepted January 30, 2000.)